International Journal of Heat and Fluid Flow 30 (2009) 356–368

Contents lists available at ScienceDirect

International Journal of Heat and Fluid Flow

journal homepage: www.elsevier.com/locate/ijhff

CFD modelling and wind tunnel validation of airflow through plant canopies using 3D canopy architecture

A. Melese Endalew [a,*], M. Hertog [a], M.A. Delele [a], K. Baetens [a], T. Persoons [b], M. Baelmans [b], H. Ramon [a], B.M. Nicolaï [a], P. Verboven [a]

[a] Faculty of Bioscience Engineering, BIOSYST – MeBioS, Katholieke Universiteit Leuven, Willem de Croylaan 42, B-3001 Leuven, Belgium
[b] Applied Mechanics and Energy Conversion Section, Department of Mechanical Engineering, Catholic University of Leuven, Celestijnenlaan 300A, B-3001 Leuven, Belgium

ARTICLE INFO

Article history:
Received 4 September 2007
Received in revised form 5 December 2008
Accepted 16 December 2008
Available online 13 January 2009

Keywords:
Canopy architecture
CFD
Canopy aerodynamics
Wind tunnel validation
Airflow

ABSTRACT

The efficiency of pesticide application to agricultural fields and the resulting environmental contamination highly depend on atmospheric airflow. A computational fluid dynamics (CFD) modelling of airflow within plant canopies using 3D canopy architecture was developed to understand the effect of the canopy to airflow. The model average air velocity was validated using experimental results in a wind tunnel with two artificial model trees of 24 cm height. Mean air velocities and their root mean square (RMS) values were measured on a vertical plane upstream and downstream sides of the trees in the tunnel using 2D hotwire anemometer after imposing a uniform air velocity of 10 m s^{-1} at the inlet. 3D virtual canopy geometries of the artificial trees were modelled and introduced into a computational fluid domain whereby airflow through the trees was simulated using Reynolds-Averaged Navier–Stokes (RANS) equations and k-ε turbulence model. There was good agreement of the average longitudinal velocity, U between the measurements and the simulation results with relative errors less than 2% for upstream and 8% for downstream sides of the trees. The accuracy of the model prediction for turbulence kinetic energy k and turbulence intensity I was acceptable within the tree height when using a roughness length (y_0 = 0.02 mm) for the surface roughness of the tree branches and by applying a source model in a porous sub-domain created around the trees. The approach was applied for full scale orchard trees in the atmospheric boundary layer (ABL) and was compared with previous approaches and works. The simulation in the ABL was made using two groups of full scale orchard trees; short (h = 3 m) with wider branching and long (h = 4 m) with narrow branching. This comparison showed good qualitative agreements on the vertical profiles of U with small local differences as expected due to the spatial disparities in tree architecture. This work was able to show airflow within and above the canopy in 3D in more details.

1. Introduction

The problem of measuring airflow in canopies has been a major issue for experimental analyses (Gross, 1987) because it is difficult and expensive to perform. For the past years several numerical approaches have been developed as a possible solution to address the experimental problem. The most widely used numerical approach to model airflow within and above plant canopies is the averaging procedure adopted by Wilson and Shaw (1977), Raupach and Shaw (1982) and Xu et al. (1997), in which the transport properties of air are averaged over a small lumped volume of the plant to remove flow details associated with individual elements. Even so, the strongly complex three-dimensional, inhomogeneous and turbulent nature of the flow within plant canopy structures and poor understanding of their interactions limited the accuracy of the prediction. Especially the modelling of the interaction between injected spray particles, airflow and the target plant canopy are far more difficult.

In the averaging procedure, there are two methods for considering the effect of the plant canopy on the airflow (Gross, 1987). In the first method the influence of trees on airflow and its turbulence is represented by closure models through additional drag force terms in the momentum and turbulence model equations. This drag force is parameterized using leaf drag area, A (m^{-1}), the dimensionless drag coefficient, C_d and sheltering factor, Sf (e.g. Wilson and Shaw, 1977; Marcolla et al., 2003). In this method A is the important parameter that determines the effects of the canopy on airflow. This parameter must be given as a three-dimensional (3D) function but only a vertical profile is usually known for different types of trees; thus this method is not always applicable (Gross, 1987). In the second method, with knowledge of the volume, V and part of it filled with leaves and branches, V, the volume poros-

* Corresponding author. Tel.: +32 16 32 23 76; fax: +32 16 32 29 55.
E-mail addresses: ayenew.melese@biw.kuleuven.be, ayenewm@yahoo.com (A.M. Endalew).

0142-727X/$ - see front matter © 2008 Elsevier Inc. All rights reserved.
doi:10.1016/j.ijheatfluidflow.2008.12.007

Nomenclature

A	plant area density (m^{-1})
C_d	drag coefficient
C_n	effective drag coefficient (m^{-1})
h	height of the trees (m)
I	turbulence intensity (%)
k	turbulence kinetic energy ($m^2\ s^{-2}$)
p	average pressure (Pa)
P	porosity
R_{ij}	Reynolds stress tensor ($m^2\ s^{-2}$)
S_ε	source term for ε ($kg\ m^{-1}\ s^{-4}$)
S_k	source term for k ($kg\ m^{-1}\ s^{-3}$)
S_u	momentum source term ($kg\ m^{-2}\ s^{-2}$)
U	average longitudinal velocity ($m\ s^{-1}$)
u^*	friction velocity in the ABL ($m\ s^{-1}$)
U_{in}	inlet air velocity ($m\ s^{-1}$)
u_i', u_j'	fluctuating velocity components ($m\ s^{-1}$)
u_i,u_j	component air velocity in x, y and z directions ($m\ s^{-1}$)
V	total volume of a sub-domain (m^3)
V_0	part of the volume filled with leaves and branches (m^3)
x_i, x_j	Cartesian coordinates (m)
y	vertical coordinate axis (m)
y_0	roughness length (m)
y^+	dimensionless wall coordinate
ε	eddy dissipation ($m^2\ s^{-3}$)
κ	Von Karman constant
ρ	density of air ($kg\ m^{-3}$)
μ	dynamic viscosity ($kg\ m^{-1}\ s^{-1}$)
μ_t	turbulent viscosity ($kg\ m^{-1}\ s^{-1}$)
δ_{ij}	the Kronecker delta
α	an attenuation coefficient

Subscripts

i, j	Cartesian coordinate index
ε, k, u	index for the source terms

ity is defined as $P = (V - V_0)/V$ whereby a weighted drag based on tree foliage density is used. However, this method also needs 3D information of the parameter P, which usually is available as single term, which limits its applicability.

In nearly all of these models horizontal homogeneity, neutral stratification and steady state conditions of the canopy structures are assumed (Wilson and Shaw, 1977; Meyers and Paw, 1986; Gross, 1987; Wilson, 1988; Ayotte et al., 1999). Even in some cases plant canopy on the ground surface is considered as a horizontally uniform bottom boundary and the influence can be imposed through the boundary roughness in which the role of the complex canopy structure on turbulent airflow around it was oversimplified (Ni, 1997). However, a natural vegetation canopy consists of an assortment of element types (branches, leaves, fruits or seeds, etc.) exhibiting a range of shapes and sizes. Furthermore, such elements are not homogeneously distributed throughout the stand but tend to be clustered and show varying density. Many of these characteristics are not treated in these models because of the complexity and the need for economy in the numerical computations. In addition to the lower accuracies (Zeng and Takahashi, 2000) due to the assumptions, the independent estimation of the three canopy parameters (A, C_d and Sf), specifically lack of any available experimental method to estimate the last two parameters is a major problem in the applications of turbulence closure models (Marcolla et al., 2003) in canopy flow. A compact tractor-mounted light detection and range (LIDAR) system used for calculating tree area density has been reported to be less suitable to crops with much smaller gap dimensions (e.g. high-density citrus trees and cereal crops) without improving the transmitter/receiver beam profile (Walklate et al., 2002).

Katul et al. (2004) indicated that second and higher order closure models are still computationally expensive and require complex numerical algorithms for three-dimensional transport problems, especially if multiple scalar species must be treated. The drawbacks and limitations of first and higher order closure models (Kaimal and Finnigan, 1994; Shaw, 1977; Wilson, 1989; Ayotte et al., 1999) and that of conventional gradient-diffusion theory (K-theory) and the transilient turbulence theory (T-theory) that have been used to study the turbulent airflow within and above plant canopy have been shown by Ni (1997), Katul and Albertson (1998) and Zeng and Takahashi (2000).

With the recent rapid advances in the speed and capacity of computers it is possible to handle complex computational models involving complex geometries, in relative ease, with reasonably short time and at fairly low computational cost. In recent years, several approaches have been developed to describe the geometric structure of plants in 3D. Some of them include structural models (Godin, 2000), functional structural models (e.g. L-systems) (Prusinkiewicz and Lindenmayer, 1996; Sievänena et al., 2000) and visualization and digitization methods (Sinoquet et al., 1997; Costes et al., 1999). No matter how much accurate methods of simulating the 3D architecture of plants are available, little or no efforts were made to link the 3D architectures of the trees with CFD to simulate air and particle or pollutant transport through the canopies.

The objective of this work was to model airflow through plant canopies by introducing a detailed 3D architecture of the canopy into CFD software and to validate the model using wind tunnel experimental results and compare with previous works and approaches. The validation was mainly based on average velocity before and after the canopies. The numerical part has two parts; (1) simulation for the wind tunnel experiment using scaled model trees, and (2) simulation in ABL using full scale trees. In its present stage this modelling is based on the numerical integration of airflow through two leafless canopies (worst case scenario for drift prediction). The model is intended to represent row planted orchard field through the use of cyclic and periodic simulations considering symmetry along the row of row planted orchard field.

2. Wind tunnel experiment

2.1. Wind tunnel

Wind tunnel experiments were carried out at the Applied Mechanics and Energy Conversion Section, Department of Mechanical Engineering of the Catholic University of Leuven. An open circuit blower type wind tunnel, which is designed to generate a uniform inlet air velocity, was used (Fig. 1). Upstream of the test section is a centrifugal blower (1), a diffuser (2), honey comb screens (3) to reduce turbulence or mean velocity variations, a settling chamber (4) and a contractor (5). Its test chamber (6) has internal dimensions of 40 cm height, 50 cm width and 200 cm length (Fig. 2). The four long sides of the test chamber were made from transparent Plexiglas. One side of the chamber was the air inlet and its opposite side was an outlet. Two scale model trees were placed at the centre of the wind tunnel test chamber as shown in Fig. 2. The trees were placed 15 cm apart from each other.

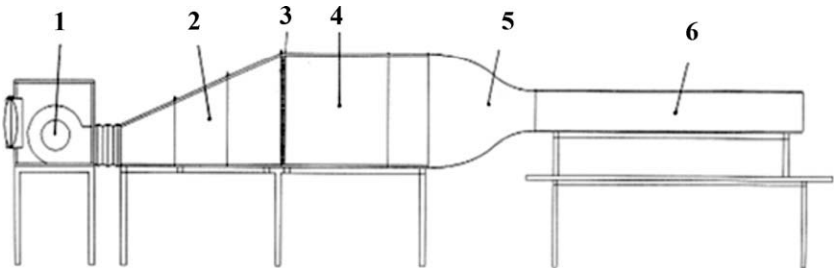

Fig. 1. Diagram of the wind tunnel for the airflow experiment: (1) centrifugal blower; (2) diffuser; (3) honeycomb grid; (4) settling chamber; (5) contractor; (6) test chamber.

2.2. Artificial scale model trees

Fig. 3a is a picture of two leafless artificial model trees made by 4D modelshop Ltd., London, UK, that were put in the wind tunnel for the experiment. The trees were made from plastic with wire-frame inside. They had an average height of 24 cm and maximum breadth of 20 cm each. The cross sections of the internodes were nearly circular with a maximum diameter of 1.25 cm for the base stem and a minimum diameter of 1 mm for the smallest branches. The surfaces of the branch stems were made rough to mimic that of real plants. The lengths of the internodes vary from 0.37 cm to 14.22 cm with mean and standard deviation of 3.28 cm and 1.84 cm. The tree branches are rigid (due to the wireframe inside) to avoid change in their structure when they are influenced by the airflow in the wind tunnel.

2.3. Experimental design

The lay out showing the position of the trees and measurement positions in the wind tunnel are given in Fig. 2. A uniform horizontal air velocity of 10 m s^{-1} was imposed at the inlet. This velocity was obtained by running the wind tunnel fan at a frequency of 39.2 Hz. The other side of the wind tunnel (the outlet) was open to the atmosphere. A stable airflow was assured in the wind tunnel by running the fan for some time before starting measurements. Velocity measurements were taken at two planes (position (A) and position (B)) in the wind tunnel (Fig. 2). Position (A) and position (B) as shown in Fig. 2 are 28 cm from the centre of the wind tunnel to upstream and downstream side respectively. Each measurement plane has three measurement points as represented by a, b and c. The measurement points are laterally 5 cm apart with each other. In each measurement point 71 vertical measurements were taken at 0.5 cm interval. Data acquisition and processing were controlled in a computer using streamWare software (Dantec Dynamics, Skovlunde, Denmark). The parameters measured simultaneously were the velocity vectors and their root mean squared (RMS) values, from which k and I were calculated.

2.4. Air velocity measurement methods

A 2D hot-wire anemometer (Dantec Dynamics, Skovlunde, Denmark) was used to measure the horizontal velocity vectors and their RMS values on the two measurement planes; position (A) and position (B) assuming the vertical component is zero. A 3D traversing system was used to hold and move the velocity probe to each measurement point vertically in the wind tunnel. Prior to using it for the actual measurements the probe was calibrated for air velocity and direction using a calibration unit of the Dantec system. For velocity calibration the unit was connected to a pressurized air supply that creates a highly stable free jet of very low turbulence. Directional calibrations were performed using a rotating holder that allows the probe to be placed in any angular position with respect to the flow. The movement of the traversing system and the operation of the calibration unit were controlled

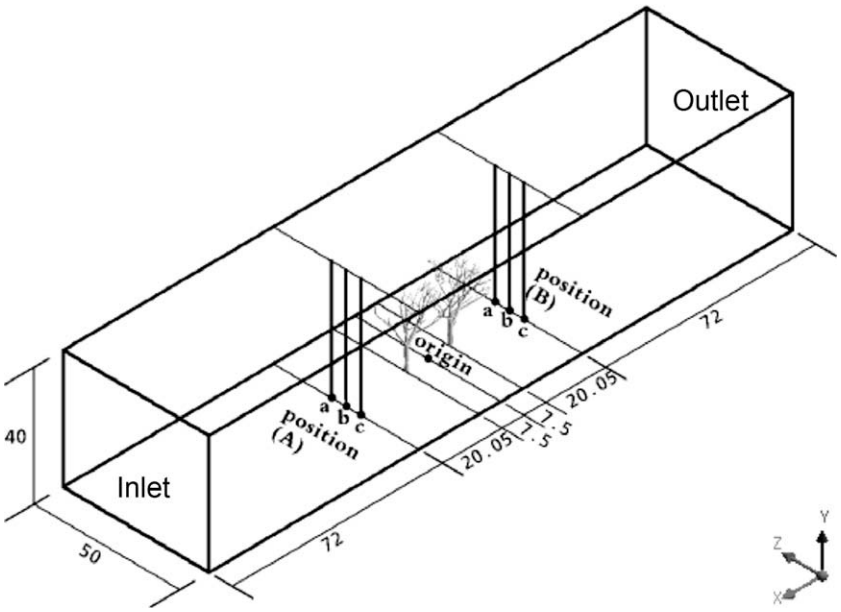

Fig. 2. Dimensions of the test chamber in the wind tunnel and layout of the positions of the trees and measurement points in the wind tunnel. All units are in cm.

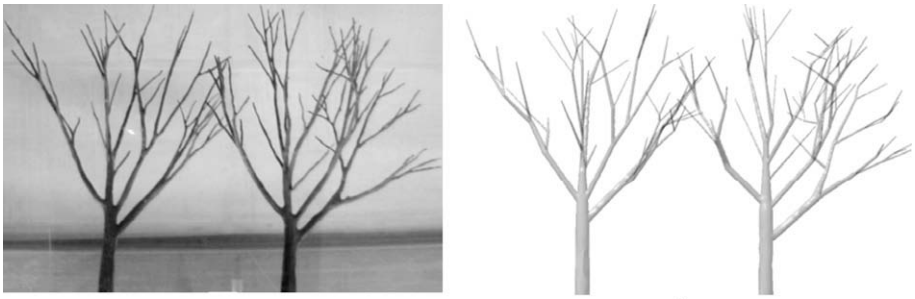

Fig. 3. Picture of the artificial trees used for wind tunnel experiment (a) and the 3D virtual geometries modelled using 'measurement and representation' method used for CFD simulation (b).

from the StreamWare application software (Dantec Dynamics, Skovlunde, Denmark) and could provide fully automatic calibrations and measurements.

3. Numerical methods

3.1. 3D architectural modelling of plant canopies

A formal mathematical description of the 'genetic construction plan' of a plant is possible due to the fact that the configurations of individual elements of plants in a genus (e.g. the branching pattern) follow relatively simple rules (Muhar, 2001). This enabled us to develop a 3D plant architectural modelling technique using internodes as building blocks of a tree. In most canopy architectural modelling, internodes are assumed as straight conical cylinders. In this work two 3D plant architectural modelling techniques were used.

The first method was used to convert the artificial trees used for the wind tunnel experiment into 3D virtual geometries using 'measurement and represention' method (Endalew et al., 2007). In this method the 3D starting and end coordinates of internodes and their diameters at the two ends were measured to represent the internodes. The starting point of an internode is the centre point where it starts to branch from a main branch and its end point is the point where another new branch starts from it unless there is an abrupt bend or curvature in that internode. If so, it is divided into two, with the point of deflection as an intersection point. The structure of the tree was developed by interconnecting these internodes together. Fig. 3b shows the artificial model trees used in the wind tunnel converted into 3D virtual geometries using this method.

The second method was used to model the architecture of the full scale orchard trees that were used for simulating airflow in the ABL. The method used a combined discrete-continuous growth simulation model which was used to develop the tree outline using plant growth parameters that are based on the environment and the properties of a tree (Table 1). In this model, time and temperature dependent continuous growth functions are described using ODEs. Simultaneously, discrete events are introduced to indicate when certain thresholds, like growth hormone (GH), are reached either to induce or inhibit growth. The life cycle of an internode starts as a bud and grows to its final length if the conditions for growth allow for this. While growing, it produces GH which is transported to its predecessor internodes to inhibit or induce the growth of other buds. At the end of its growth, it generates a new active apical bud that continues growing with a number of (dormant) side buds. All side buds remain dormant waiting for their time to come (if ever) to become active and start growing depending on the GH threshold level. The growth cycle starts over again for each newly generated bud. More details of this model are given by Endalew et al. (2006).

GH turnover within and between a growing bud and a grown internode controls the growth. This is an endogenous growth control mechanism whereby the hormone balance is affected by exogenous mechanisms; *seasonal temperature changes* which affect hormone production rate and *pruning activities* that are inducing a new burst of growth. Yearly temperature is simulated assuming a sinusoidal pattern. Some of the input parameters used in this modelling are given in Table 1.

This modelling approach has two phases; first it generates a 3D outline of the tree by connecting internode centrelines and then it forms the solid tree by building conical bodies around these lines. The 3D starting and end coordinates of the internodes are calculated using straight forward trigonometric relationships using the branching angle and the final length of the internode. The first phase of this 3D architectural modelling technique was implemented using Prosim (Prosim bv, Zoetermeer, NL). Prosim is a software environment for combined discrete-continuous modelling and simulation.

For both canopy architectural modelling techniques the 3D structure of the trees from interconnected conical cylinder internodes were made in ANSYS 5.7.1 (ANSYS Inc., Canonsburg, PA, USA). The coordinate and diameter data were converted into a script file which, when read in ANSYS 5.7.1, it generated 3D sold tree geometries. Fig. 3b shows the 3D virtual geometries of the artificial trees obtained by the 'measurement and representation' method which were used for the simulation of the wind tunnel experiment. Fig. 4a and b are 3D geometries of trees obtained using the second combined discrete-continuous architectural modelling method that were used for simulation in the ABL. The difference in the shapes of the trees in Fig. 4a and b was due to the difference in the growth parameters applied (Table 1). G1 are groups of trees generated with shorter maximum internodes (300 mm), slower

Table 1
Some of the growth parameters and their values that are used to generate G1 and G2 trees using the combined discrete-continuous plant growth model.

Growth parameters	Values	
	G1	G2
Simulation time (years)	7	7
Maximum stem radius (mm)	70	70
Minimum (final) branch radius (mm)	5	5
Maximum internode length (mm)	*300*	*400*
Starting length of an internode (mm)	0.02	0.02
Growth rate of an internode (mm/day)	*0.034*	*0.05*
Activation energy for growth	15,000	15,000
Reference growth temperature (°C)	15	15
Hormone exchange rate between Internodes	0.4	0.4
Number of side buds per node	1	1
Critical hormone level for growth initiation	0.04	0.04
Average growth angle (radians)	*0.2*	*0.08*

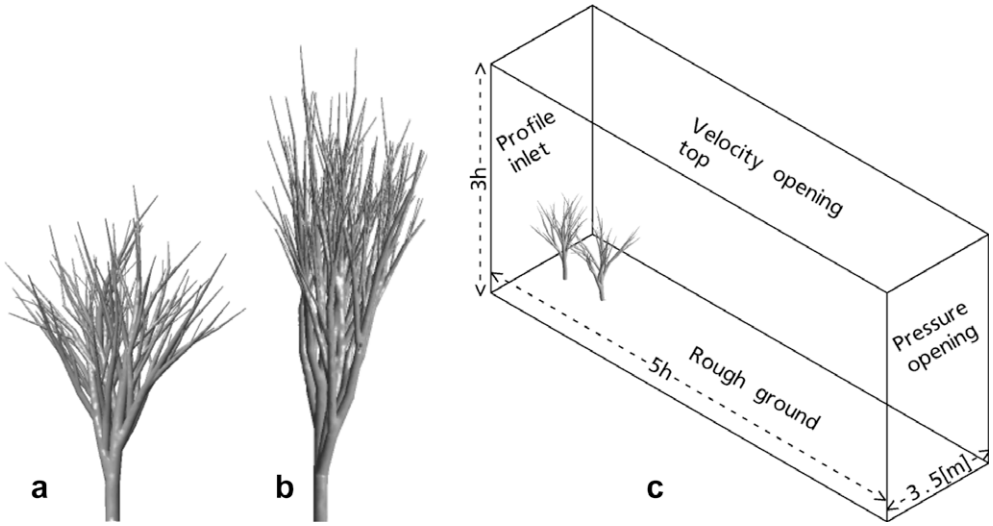

Fig. 4. Two groups of trees (a) short with wider or sparse branching (G1), (b) long with narrow or dense branching (G2) and (c) simulation domain and boundary conditions for cyclic simulation with G1 inside.

growth rate (0.034 mm day^{-1}) and wider branching angle (0.2 radians) as shown in Fig. 4a. Whereas G2 are those generated with longer maximum internodes (400 mm), faster growth rate (0.05 mm day^{-1}) and narrower branching angle (0.08 radians) pattern (Fig. 4b) (Table 1).

3.2. Simulation domain and boundary conditions

Three groups of simulations were made in this work; one with the trees used in the wind tunnel, two with trees in the ABL. The domain for the wind tunnel simulation has the same dimensions as that of the wind tunnel experimental set up (Fig. 2) with trees of Fig. 3b. In the ABL cyclic and periodic simulations were made each with G1 (Fig. 4a) and G2 (Fig. 4b) trees inside the domain as shown in Fig. 4c for G1. The size of the domain for these simulations is function of the tree height, h.

For simulation with scaled model trees in the wind tunnel a fluid domain with inner dimensions equal to the wind tunnel was used. The two 3D virtual tree geometries shown in Fig. 3b were placed in the domain centre on the bottom no-slip wall boundary with 15 cm gap between them along the length. The trees were placed 15 cm apart in the domain (Fig. 2). This placement of the trees considers the average interplant spacing of 1.5 m in a row of an orchard when it is scaled up ten times. Except the inlet and the outlet, all the parts of the domain were set as no slip wall boundary condition as this was the case in the wind tunnel. At the inlet a uniform air velocity of 10 m s^{-1} was imposed. The opposite side of the inlet, i.e. the outlet was set as a pressure outlet with a zero relative pressure. Based on the calculation I from the RMS values of the velocity vectors measured at the inlet, a low intensity of 1% was used for turbulence at the inlet. As the recent work of Lam and Lin (2008) on flow around wavy cylinders and Faruquee et al. (2007) on the effects of axis ratio on laminar fluid flow around an elliptical cylinder used, no slip wall boundaries were used for the solid virtual trees in the domain. The surfaces of the tree stem and branches used for the wind tunnel were not smooth. Since there is no information in the literature on the surface roughness of plant stems and branches a roughness length (y_0) of concrete which is equal to 0.2 mm (Wieringa, 1992) was used as a reference to represent the surface roughness of full scale trees. Since the wind tunnel trees are about 10 times smaller than the average size of full scale trees, a reference y_0 value of 0.02 mm was used for trees used in the wind tunnel.

For simulation with full scale trees in the ABL the size of the domain for cyclic simulation had a height of 3h, a length of 5h and a width of an average inter-row spacing of orchard field (3.5 m); where h is the average height of the trees. Thus, the domain with G1 (shorter trees of 3 m height, Fig. 4a) had 9 m height, 15 m length (Fig. 4c) and that with G2 (longer trees of 4 m height, Fig. 4b) had 12 m height and 20 m length. The width of the domains with both G1 and G2 had a width of 3.5 m. The bottom of the domains was set as rough ground with a roughness length (y_0 = 0.005 m) assuming that under the trees there are no noticeable obstacles (Wieringa, 1992). Considering an orchard field with row planted crops is symmetric along the row, the two planes along the row were set as symmetry boundaries. The top and the end of the domain were Cartesian velocity and pressure openings, respectively. A profile U, ε and constant k were imposed at the inlet. Simulations were made at a reference wind velocity at h, $U(h)$ of 3 m s^{-1} and 5 m s^{-1} and the results were normalized with the friction velocity in the ABL. A roughness based logarithmic velocity profile, a constant k and vertical profile of its eddy dissipation, ε imposed in this boundary are given in the equations below.

$$U(y) = \frac{u_*}{\kappa} \ln\left(\frac{y + y_0}{y_0}\right) \tag{1}$$

$$k = \frac{u_*^2}{\sqrt{C_\mu}} \tag{2}$$

$$\varepsilon = \frac{u_*^3}{\kappa(y + y_0)} \tag{3}$$

where $U(y)$ is the mean air velocity at height y (m s^{-1}), u^* friction velocity in the ABL which can be calculated at $U(h)$ (m s^{-1}), κ Von Karman constant (=0.41), y_0 aerodynamic roughness length (m), k the turbulent kinetic energy (m^2 s^{-2}) and C_μ is k-ε turbulence model constant (=0.09). The domain and its boundaries for cyclic simulation are shown in Fig. 4c. In the cyclic simulation the result of a simulation near the second tree at wake side is taken and recycled as an inlet for the next simulation. The recycling continued until the change in the results of consecutive simulations became insignificant.

The domain for periodic simulation had the same heights and widths as the cyclic simulation but the length was twice an inter plant spacing for orchards (2 × 1.75 m = 3.5 m) for both groups of trees in the domain. For this simulation all the boundaries were the same as the cyclic simulation but the inlet and the outlet were

set as translational periodic boundaries with a canopy roughness profile of U, k and ε used as initial conditions.

For both cyclic and periodic simulations two trees of the same group were put in the domain close to the inlet with a gap of 1.75 m in between. The surfaces of the tree branches in all cases were assumed no slip wall boundaries.

3.3. Model governing equations

The CFD code used for this modelling was ANSYS CFX-10.0 (ANSYS Inc., Canonsburg, PA, USA). The set of equations solved by ANSYS CFX-10 are the Reynolds-averaged Navier–Stokes (RANS) equations in their conservation form. The steady state three-dimensional RANS equations of mass and momentum conservation for an incompressible, viscous, isothermal flow of a Newtonian fluid, in Cartesian coordinates, in partial differential equation and conservation form with the Boussinesq's hypothesis are given by (e.g. Launder and Spalding, 1994; Versteeg and Malalasekera, 1995; Cheng et al., 2003);

$$\frac{\partial(u_i)}{\partial x_i} = 0 \tag{4}$$

$$\rho\frac{\partial u_i u_j}{\partial x_j} = -\frac{\partial p}{\partial x_i} + \frac{\partial}{\partial x_j}\mu\left(\frac{\partial u_i}{\partial x_j} + \frac{\partial u_j}{\partial x_i}\right) - \rho\frac{\partial}{\partial x_j}(\overline{u_i' u_j'}) \tag{5}$$

where u_i is the ith component of the averaged air velocity (m s^{-1}), p is the average pressure (Pa), ρ is the density of air which is assumed constant (kg m^{-3}), x_i and x_j Cartesian coordinates, μ is the dynamic viscosity (kg m^{-1} s^{-1}), u_i' and u_j' fluctuating velocity parts (m s^{-1}). The indexes i and j are used to distinguish Cartesian components ($i, j \varepsilon \{1, 2, 3\}$); if an index appears twice in a term, summation over that index is required. The turbulent Reynolds stress tensor, $\overline{u_i' u_j'}$ in Eq. (5) is modelled by adopting the extended Boussinesq hypothesis (Versteeg and Malalasekera, 1995), which relates the turbulent stresses to the mean rate of deformation:

$$\overline{u_i' u_j'} = -\frac{\mu_t}{\rho}\left(\frac{\partial u_i}{\partial x_j} + \frac{\partial u_j}{\partial x_i}\right) + \frac{2}{3}k\delta_{ij} \tag{6}$$

where μ_t is the turbulent viscosity (kg m^{-1} s^{-1}) and δ_{ij} the Kronecker delta ($\delta_{ij} = 1$ if $i = j$ and $\delta_{ij} = 0$ if $i \neq j$). k for the experiment was calculated from the RMS values (u_i') as:

$$k = \frac{1}{2}(\overline{u_i' u_i'}) \tag{7}$$

The turbulence intensity I in% was calculated from k and average longitudinal velocity U as:

$$I = 100\left(\sqrt{\frac{2}{3}\frac{k}{U^2}}\right) \tag{8}$$

To compare the present approach with the previous ones with the averaging procedure adopted by Wilson and Shaw (1977) the region with the canopies in the wind tunnel was replaced by rectangular porous sub-domain instead of the complex 3D tree geometries. In this sub-domain source and sink terms as proposed by Sanz (2003) and used by Katul et al. (2004) and Da Silva et al. (2006) were added to the momentum and energy equations to represent the effect of the entire canopy to airflow. The term, S_u was added as a sink term in the momentum equation and those of S_k and S_ε as source terms in the turbulent kinetic energy and eddy dissipation equations of the turbulence model, respectively. Neglecting viscous drag relative to form drag (Sanz, 2003), S_u is modelled as:

$$S_u = -\rho C_d A U^2 = -\frac{1}{2}\rho C_n U^2 \tag{9}$$

For most leafed vegetation, the drag coefficient, C_d (≈0.1–0.5), and the leaf area density, A (m^{-1}) varies appreciably with vertical height (Katul et al., 2004). But in this case, since we use leafless trees the term $2C_dA$ was taken as form drag coefficient (C_n), which depends on one sided vegetation surface density, A (Sanz, 2003). According to the approach of Da Silva et al. (2006), the average vertical profile of ($C_n(y)$) was calculated from the velocities measured before and after the canopy horizontally averaged at position (A) and position (B) of Fig. 2 at each vertical point of measurement. The average measured velocities on position (B) were lower than in position (A). This velocity decline through the canopy due to momentum absorption was modelled as exponential function of C_n and A (Da Silva et al., 2006), given by;

$$U_B(y) = U_A(y)\exp(-C_n(y)Ay) \tag{10}$$

where $U_A(y)$ and $U_B(y)$ are the horizontal averaged velocities at a given position y at position (A) and position (B) (see Fig. 2), respectively. With L (m), the depth of the canopy along the wind tunnel that both the trees occupy between position (A) and position (B), which is 0.56 m in this case, the value of C_n is given by;

$$C_n(y) = \frac{1}{LA}\ln\frac{U_A(y)}{U_B(y)} \tag{11}$$

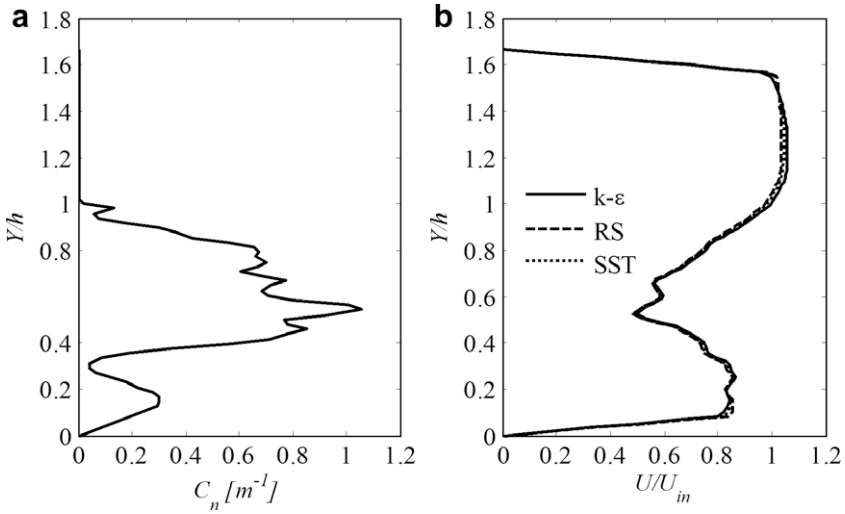

Fig. 5. Vertical profiles of (a) the effective drag coefficient (C_n) as calculated using Eq. (11) and (b) simulation results of the vertical profiles of normalized U at point b of position (B) obtained from the different turbulence models.

The value of the frontal area density, A was obtained from the ratio of one sided surface area of the trees as calculated from their detailed 3D architecture to the average volume that the two trees occupy. The vertical profile of C_n as calculated using Eq. (11)is shown in Fig. 5a.

The source terms, S_k and S_ε occur due to the fact that vegetation elements disturb the continuity of the mean flow motion and generate wake turbulence ($\approx C_n U^3$) that dissipates rapidly (Raupach and Shaw, 1982) often leading to a 'short-circuiting' of the Kolmogorov cascade (Kaimal and Finnigan, 1994; Poggi et al., 2004). In the k and ε equations the source terms S_k and S_ε as simplified by Walklate et al. (1996) are given by:

$$S_k = \frac{1}{2}\rho C_n k U \tag{12}$$

S_ε is less known and the proposed formulations are mainly based on a standard dimensional analysis (Katul et al., 2004). The expression used in our work was:

$$S_\varepsilon = \frac{1}{2}\rho C_n \varepsilon U \tag{13}$$

3.4. Turbulence model

A comparison was made between three turbulent models; k-ε, shear stress transport (SST) and Reynolds stress (RS) model to see whether or not the presence of the complex canopy structures in the domain could influence the results obtained and the convergence when using different turbulence models and to select an appropriate turbulence model for the validation work. In the SST and k-ε turbulence models the solution converged faster than the RS model to normalized (RMS) residuals of less than 10^{-7}. In the RS not only the convergence was slow but also it was poor with final RMS residuals of 10^{-4}. However, as shown in Fig. 5b the vertical velocity profiles in the wake region at point b of position (B) (Fig. 2) revealed that there was no significant difference between the profiles computed with the three different turbulence models.

While the standard k-ε two equation model provides good predictions for many flows of engineering interest because of its robustness, economy and reasonable accuracy, a Reynolds Stress model may be more appropriate for flows with sudden changes in strain rate or rotating flows, and the SST model may be more appropriate for separated flows for it uses the turbulence/frequency-based model (k-ω) at the wall and k-ε in the bulk flow. Because of its stability and numerical robustness the k-ε model was used for validation and for the rest of the simulations. In several commercial CFD soft ware packages, the two equation k-ε turbulence model is the most popular and widely used model for engineering and industrial applications (Katul et al., 2004) as well as in several spray models (e.g. Brown and Sidhamed, 2001; Da Silva et al., 2006). The equations of k-ε turbulence model supplemented by additional source and sink terms were used by several authors (e.g. Gross, 1987; Lee, 2000; Da Silva et al., 2006) for modelling airflow through plant canopies and yet its application to model turbulent flow in plant canopies has not given comparable attention. This may be due to the fact that the parameterizations of the additional source (and/or sink) terms in the closure models remains uncertain (Sanz, 2003). The k-ε turbulence equations supplemented by additional source and sink terms used in previous models involve spatial averaging of the vegetation canopy to avoid the flow details within the individual plant elements (e.g. Wilson and Shaw, 1977). In the averaging procedure much information is lost which might be costly with regard to loss of information at the level of individual canopy elements which is important in spray modelling. Here, since a 3D canopy structure which mimics the real effects of the canopy elements and yet allows the use of CFD solvers was introduced into the domain, k-ε turbulence model was used without source or sink terms. This will give an opportunity to address the problem related to the uncertainty in the parameterization of the sink and source terms. This approach was also compared with the classical approach using source and sink terms of Eqs. (11)–(13) to show its advantage on the three dimensionality of the results.

3.5. Meshing and solution procedure

The computational fluid domain was discretized using an unstructured tetrahedral control volume mesh. The global mesh size in the domain and near the surface of smallest tree branches was resolved based on the minimum dimensionless distance from the wall or the location of the wall adjacent cell (y^+) value, with a main target to obtain the desired level of accuracy and flow details near each element of the tree. To attain the desired mesh a minimum edge length was defined on the surface of the smallest canopy branches which reduces to the maximum free space global edge length in eight layers. Around the surfaces of the smallest branches at least five layers of tetrahedral elements were assured to get enough details of airflow around the branches. A mesh sensitivity study was done to apply an optimum mesh size for the work.

The global mesh sizes in the domain and smallest edge length on the surface of the smallest branches, the total number of elements and nodes obtained and the convergence time required to solve the turbulence and momentum equations (total CPU time) for each mesh size are given in Table 2. Since we expect more variability in the velocity magnitude in the wake region due to the effect of the trees, the longitudinal velocity U averaged at position (B) was used for comparison. Except near the wall boundaries for the mesh with global size of 5 cm, all the mesh sizes gave similar vertical profiles of U. Among the mesh sizes that gave similar results in the wake velocity, the one with 4 cm global mesh size which gave a smaller number of tetrahedral elements and required less CPU time (Table 2) than the other two sizes (2 cm and 3 cm) was selected for the rest of the validation work.

Based on the mesh sensitivity study, a free space global mesh size of 4 cm with a minimum edge length of 0.1 mm on the surface of the thinnest branch which reduces to the maximum global edge length in eight layers was selected to compare with the measurements. This mesh setting gave 2,172,114 tetrahedral elements uniformly distributed over the domain with a total number of 396,600 nodes. The solution of all equations converged to a normalized (RMS) residual of less than 10^{-7} in 500 iterations. This calculation took a total CPU time of about 27 h on an Intel Pentium IV, 3 GHz Win2002 workstation with 1 GB of RAM (Table 2).

The same meshing procedure was followed for the simulation that was done with the full scale orchard trees in the ABL with the meshing parameters proportionally scaled based on the size of the trees.

Table 2
Mesh statistics and convergence time for different mesh size and turbulence models.

Mesh size (cm)		Total number		Total CPU time in hours after 500 iterations	
Global	Smallest	Elements	Nodes	k-ε/SST	SSG-RS
5	0.01	2,103,397	384,853	26.15	32.75
4	0.01	2,172,114	396,600	27.15	41.57
3	0.0075	2,232,433	407,725	27.74	46.86
2	0.0075	2,699,055	489,411	42.31	54.65

4. Results and discussion

4.1. Profiles of mean air velocities

Normalized vertical profiles of average longitudinal air velocity, U measured in the wind tunnel and obtained by simulation using the 3D canopies in the domain and source sink terms in a porous sub-domain were compared on the vertical planes of position (A) and position (B) of Fig. 2. U was normalized with the uniform inlet velocity (U_{in}) and the vertical axis (Y) was normalized with the average tree height (h = 24 cm). The surfaces of the artificial trees stems and branches used in the wind tunnel were not smooth. Assuming the flow over the surfaces of the branches is continuous for a very thin layer of very fine roughness for short time, a scalable wall function of ANSY-CFX was used to capture the flow near the surfaces of the tree branches. Comparisons of the measurements were made with simulations with the surfaces of the tree branches set as no slip smooth and rough (for y_0 = 0.01 mm, 0.02 mm and 0.03 mm) wall boundaries.

In position (A) the vertical profiles of U at points a, b and c were the same. In this position both the models well represented the measured values with all average RMS, mean absolute and percent errors less than 0.2, 0.011 and 1.1%, respectively (Table 3). The accuracy of the model at this upstream position was quite good.

In position (B), at the wake, the normalized vertical velocity profiles (Fig. 6) were more disturbed as expected due to the high influence of the trees on the airflow. In Fig. 6 the profiles shown in (a), (b) and (c) are those for points a, b and c of position (B), respectively (refer Fig. 2). Whereas the last graph at the right bottom corner is the average across the plane at position (B). When using the 3D tree architecture, qualitatively the shapes of the simulated profiles were similar to that of the measured ones and quantitatively the simulated results also represented the measured values well with all average RMS, absolute and percent errors less

Table 3
errors in predicted U at position (A) and position (B) for the trees as smooth and rough wall boundaries.

Position	Measurement points	Root-mean-square errors Branches		Mean absolute errors Branches		% Errors Branches	
		Smooth	Rough[a]	Smooth	Rough[a]	Smooth	Rough[a]
(A)	a	0.129	0.116	0.006	0.006	0.604	0.585
	b	0.202	0.121	0.011	0.009	1.175	0.921
	c	0.111	0.200	0.006	0.007	0.588	0.745
	average	**0.147**	**0.146**	**0.008**	**0.007**	**0.789**	**0.751**
(B)	a	0.241	0.271	0.018	0.020	1.741	1.905
	b	0.604	0.795	0.040	0.054	6.018	7.759
	c	0.545	0.825	0.043	0.058	4.625	6.601
	average	**0.463**	**0.631**	**0.034**	**0.044**	**4.128**	**5.422**

[a] The roughness value, y_0 used here is y_0 = 0.02 mm.

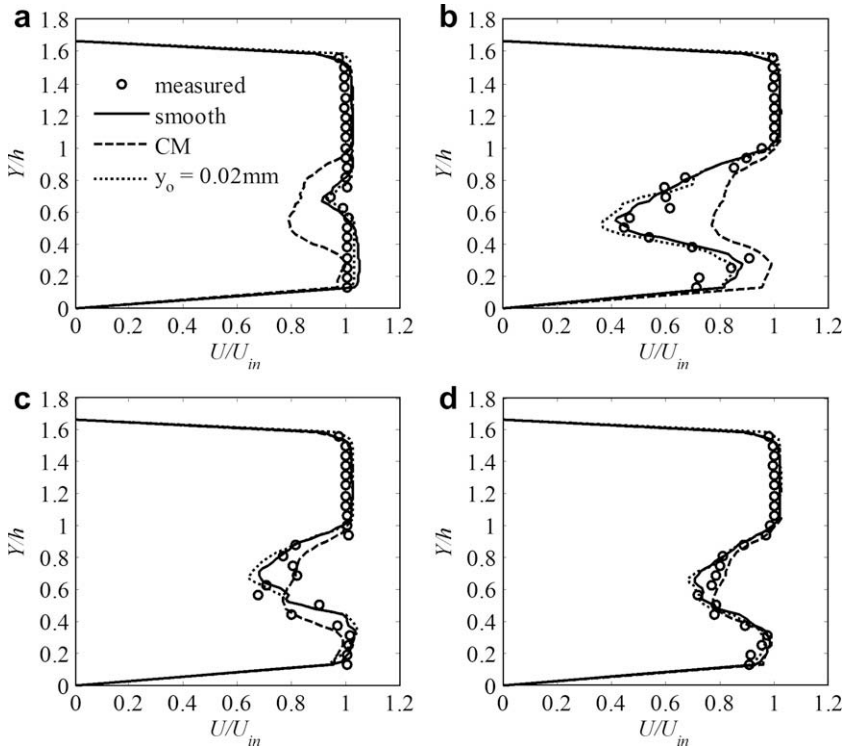

Fig. 6. Vertical profiles of normalized U on position (B) at points a, b, c and average over the plane across position (B), respectively; (**– – –**) and (·····) simulated with the trees as smooth and rough (y_0 = 0.02 mm) surfaces respectively, (————) simulated with sink-source terms of Eqs. (9), (12), and (13) in the porous sub-domain that represents the region occupying the trees and (**O**) measured values.

than 0.83%, 0.06% and 8% as shown in Table 3. The simulation with the trees as rough surfaces under predicted U at the wake as compared with those simulated with the trees as smooth surfaces. The under prediction was higher in the denser regions of the canopy but the differences were not significant. Moreover, with the classical approach there was a significant under prediction of the average velocity in the sparse regions of the canopy (Fig. 6a) and a vice versa in the denser regions (Fig. 6b) while the accuracy of the average at position (B) quite comparable with both the present approach and the measurements (Fig. 6 (average)). Generally the results with the trees as smooth surfaces gave better accuracy in U (Table 3). Looking at the velocity profiles in Fig. 6 and velocity contour in Fig. 7, it was observed that the air velocity was generally higher on the two sides and the top of the trees due to the resistance of the trees in the middle. Specifically, within the canopy there is overflow and speed up of air around the tree elements to compensate for the resistance by the tree elements (Fig. 7). On average basis the results of the classical approach were acceptable but gave the same velocity profiles downstream across the plane behind the trees. This is due to the assumption of horizontal homogeneity which is not the case in real situation. With the present approach the horizontal differences in the vertical profiles of U, as shown in Fig. 6a–c were well predicted and showed the horizontal inhomogeneity which represents the real situation.

4.2. Profiles of turbulence kinetic energy and turbulence intensity

The vertical profiles of k and I on the two measurement planes (position (A) and position (B)) in the wind tunnel were compared with the simulation results. The observed k was calculated from the RMS values of the velocity vectors using Eq. (7) and was normalized by the square of the uniform inlet velocity (U_{in}). I was also calculated from k and U using Eq. (8). For k and I the measurements were compared with simulations obtained from the trees with smooth or rough no slip surfaces (with different y_0 values) as well as with simulations using source terms of Eqs. (12) and (13) in porous sub-domain created around the solid tree parts to capture the average turbulence in the region. The simulation with the porous sub-domain around the tree elements is different from the classical approach which uses totally a porous sub-domain for the entire region occupied by the canopy. Here cylindrical sub-domains were created around each element of the tree. They were merged together as one porous domain while the 3D virtual canopies are still there in the sub-domain. The surfaces of the trees in this approach were considered as smooth wall. The parameter that needed to be changed for this approach was C_n. For the full closure model C_n was obtained from the approach described in Section 3.3, but in this approach it was determined using a trial and error approach until the simulations produced good agreement with the measurements (Wilson and Shaw, 1977).

In position (A) (refer Fig. 2) at all points the model represented the measured values well within the canopy height, h both with and without including tree surface roughness. The average I in this region was about 1%. In Fig. 8 only the profiles of k and I at the most disturbed wake region of position (B) at measurement point b and c are presented because the results at the other points showed similar behaviour and the prediction was more accurate than these points. In this region due to the influence of the canopy I in the denser regions was even greater than 10% but above h and in sparse canopy regions the intensity was lower. In this region the simulations with the trees as rough surface (y_0 = 0.02 mm) and that with the source terms in the porous sub-domain around the branches (CM) represented the measured values within h better than that with the trees as smooth surfaces and other roughness values. With smooth and y_0 = 0.01 mm there was under prediction of k and I but there was over prediction for y_0 = 0.03 mm. As Fig. 8 shows both k and I increased in the dense canopy regions as the frictional resistance from canopy elements cause additional turbulence in the airflow within and around the trees. Generally there was an over estimation of both k and I with both approaches except for smooth wall and y_0 = 0.01 mm. Furthermore, close to the ground there was poor representation of the measurements by the model. Although the increase in k and I with canopy density within the canopy height was reasonably well predicted, differences between the measured and predicted values of k and I were more significant than that of U. A possible reason for this could be k-ε turbulence models from RANS equations do not capture the highly fluctuating velocity components expected to occur in this region. This could be due to the fact that the model assumptions and constants that were meant to be used in the averaging proce-

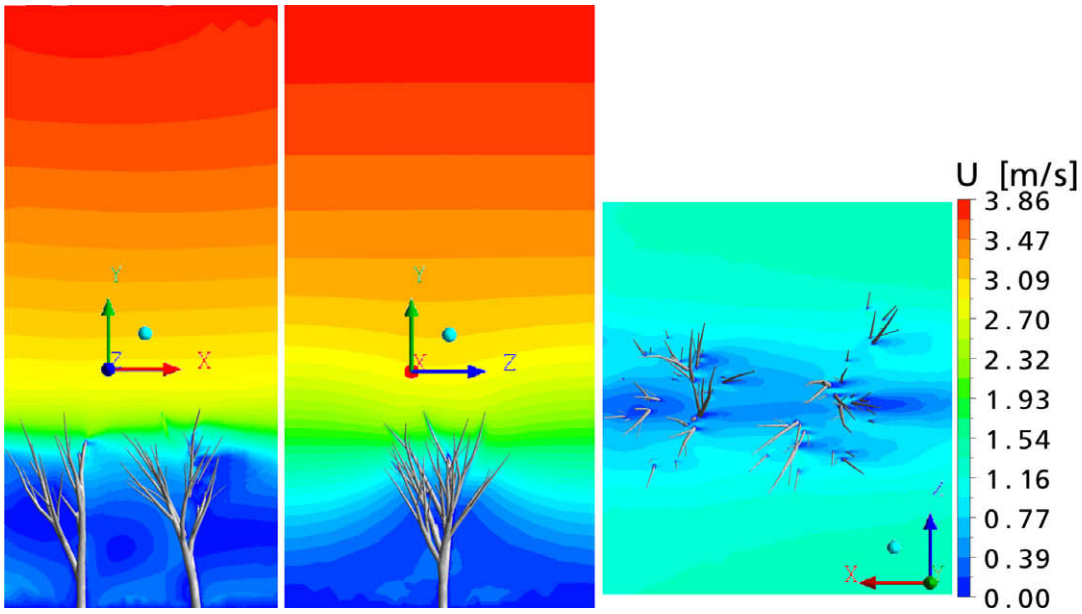

Fig. 7. Velocity contour plots on vertical plans through the trees (left) and horizontal plane at 1.75 m from the ground (right) captured from simulation using full scale trees with $U(h) = 3\ \mathrm{m\ s^{-1}}$.

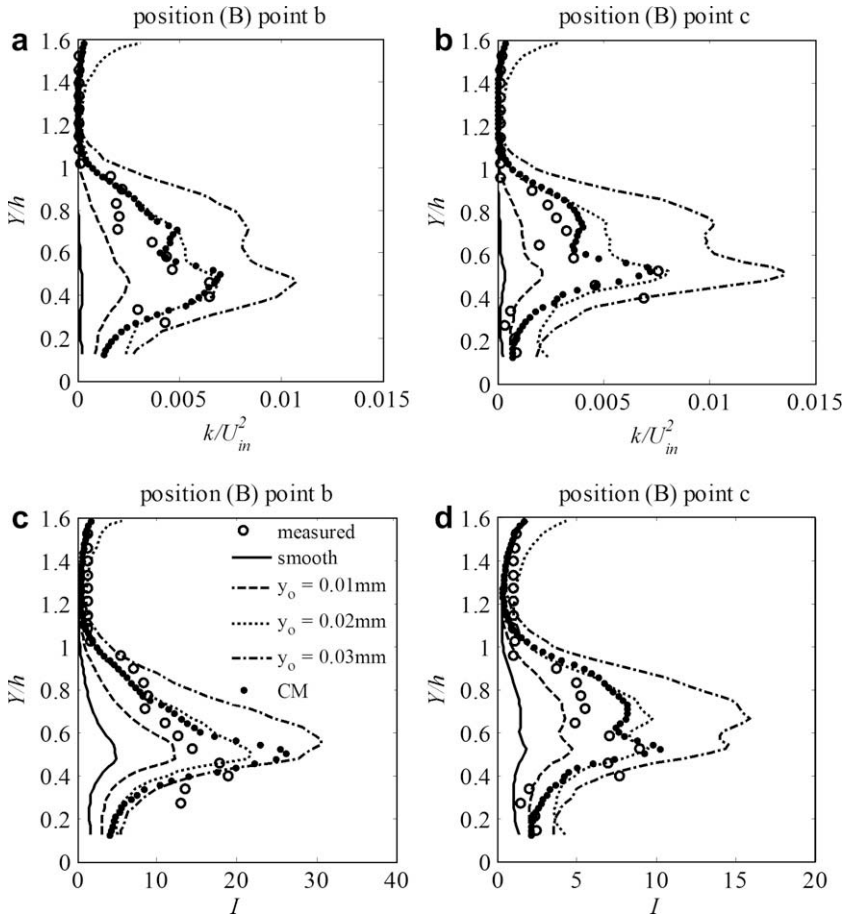

Fig. 8. Vertical profiles of normalized k (a) and (b) and I (%) (c) and (d) at measurement point b and c of position (B), respectively; the legend on (c) works also for (a), (b) and (d). CM represents the results obtained using source terms for k and ε using Eqs. (12) and (13) in the porous sub-domain created around the tree elements.

dure may not fully work and represent the measured values in the wind tunnel when they are used in the present approach where the canopy detailed geometry is resolved in the model. They should be modified and studied further to be used in the present approach. The difference might also be due to the unresolved parameterizations of wall roughness and source terms.

4.3. Airflow profiles and k within full scale canopies in the ABL

Despite the difficulties in determining the typical patterns of airflow within vegetation canopies due to the complex airflow dynamics determined by the spatial variability of the canopy elements, many observations of the vertical profile of U within ABL appear in the literature (e.g. De Bruin and Moore, 1985). Since it was not possible to generate the ABL above the trees in the wind tunnel, cyclic and periodic simulation of air velocities were carried out using full scale orchard canopies giving enough free space above the canopies to create the boundary layer. To ensure that the approach is repeatable for different shape and density of trees with different spatial structures, comparison was made between two groups of trees G1 and G2. The two groups of trees were obtained by changing some of the growth parameters (Table 1) of the combined discrete-continuous plant architectural modelling method described in Section 3.1. The first groups of trees (G1) were short (3 m) with wider or sparse branching pattern (Fig. 4a) and the second groups of trees (G2) were long (4 m) with narrower or dense branching pattern (Fig. 4b). The results were qualitatively compared with each other and with other works in the area (Gross, 1987; Cionco and Ellefsen, 1998; Albertson et al., 2001, Zeng and Takahashi, 2000; Pyles et al., 2004) to see whether or not tree shape and density can change the normalized vertical velocity profiles.

Fig. 9a shows the normalized vertical velocity profiles of cyclic and periodic simulation results as compared with the profile for canopy roughness (Cionco and Ellefsen, 1998), calculated using analytical formulas for the three regions and Albertson (Albertson et al., 2001). In this figure it was shown that the results of the periodic simulation perfectly matched with Albertson (Albertson et al., 2001) whereas results of cyclic simulation marched more with profile of canopy roughness (Cionco and Ellefsen, 1998) and calculated. In this case U was normalized with the friction velocity (u^*) within the ABL and vertical height y was normalized with tree height (h). The profile by Cionco and Ellefsen (1998) is a general vertical velocity profile expected for a canopy roughness. The profile from Albertson et al. (2001) is a profile within and above a vertical shape of a pine forest with an average height of 14 m. The profiles of both cyclic and periodic simulations being acceptable, it was observed that the periodic simulations gave lower velocities than the cyclic simulation within h. Though the periodic approach is computationally less demanding, its results are highly dependent on initial conditions. On the other hand, the cyclic simulation, despite its computational demand, it has the advantage of giving more space for setting realistic boundaries to get realistic results.

Fig. 9b shows the simulation results of air velocity profiles using the two groups of trees (G1 and G2) to show the effects of tree shape and density on airflow as compared with profiles for canopy roughness and calculated similar to Fig. 9a. The log profile shown in Fig. 9 was calculated using Eq. (1). As Fig. 9b illustrates the vertical profile

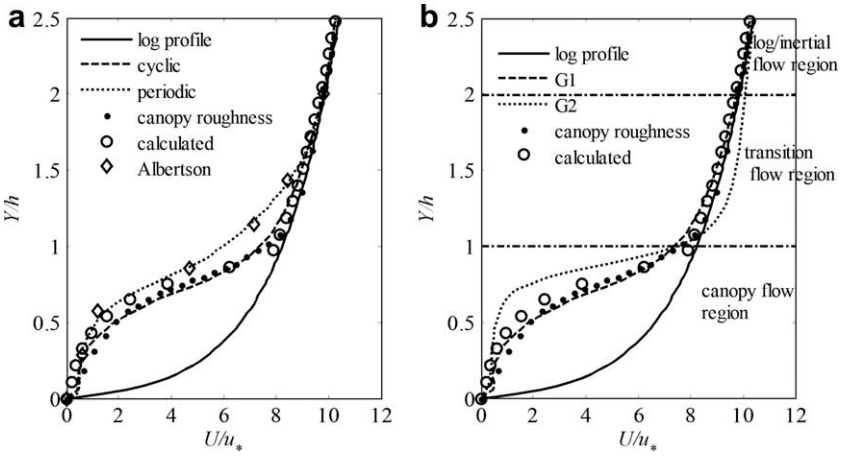

Fig. 9. Normalized vertical profiles of U obtained (a) by cyclic and periodic simulations using G1 and (b) by cyclic simulation using G1 and G2. (a) is to show the differences between cyclic and periodic simulations and (b) is to show the effects of canopy density both compared with calculated results, profiles of canopy roughness and other works showing the three flow regions.

of U reached the log profile at $2h$ with G1 whereas with G2 the profile reached the log profile above $2h$. This showed how canopy density can affect the aerodynamics above canopy roughness. The velocity profiles qualitatively agree well with the other works compared with and quantitatively have similar explanations as (Gross, 1987; Zeng and Takahashi, 2000; Albertson et al., 2001). Zeng and Takahashi (2000) showed the effects of foliage density on the vertical wind profile in rubber tree plantation during fully leafed, partially leafed and leafless periods. In their work they found that an increase in foliage density results in air velocity decrease in the lower canopy and increase above the canopy, because it is easier for momentum to penetrate the canopy if the canopy is thin. The same conclusion was also made by Albertson et al. (2001). Gross (1987) showed the effect of canopy shape on wind profile using ball and cone shaped trees. He indicated that the shape of the canopy is the dominant factor determining the flow field.

Below $2h$, although the general shapes of the profiles were similar, there were some quantitative differences. These differences were expected to be due to the spatial variability of the trees (height, foliage density and shape). Since the trees in G2 were denser than G1 more air tends to flow around and above the trees than within the canopy. These phenomena gave a tendency for the profile with G2 to bulge inward below h and outward above h and it took longer for it to reach the log profile (at >$2h$).

From velocity profiles in Fig. 9 it could be observed that the frictional resistance from a vegetation canopy causes local difference in airflow around and within the canopy. Mostly such plant canopy effects are felt from the ground up to twice (or more) the canopy height and this is known as the roughness sub-layer (Georgiadis et al., 1996; Ni, 1997). Due to the complex patterns of the individual tree elements, the airflow in the roughness sub-layer is strongly three-dimensional and complex. According to Georgiadis et al. (1996) this roughness sublayer is divided into three regions.

The first region called the *canopy flow region* is a region from the ground to the canopy height h. This region is highly influenced by the canopy characterized by a reduction in the average velocity (Fig. 9) and an increase in fluctuating components which favours increase in turbulence kinetic energy and intensity (Fig. 8) in the wake regions. In this region the airflow can be described by the exponential relationship given by Cionco (1972):

$$U(y) = U(h)\exp\left[\alpha\left(\frac{y}{h}-1\right)\right] \tag{14}$$

where α is an attenuation coefficient. It is canopy dependent and defines the slope of the log linear profile of the velocity in this region.

The second region just above the canopy is called *transition flow region*. The vertical velocity profile in this region significantly varies between the upper inertial and the inner canopy flow region and the depth of this layer is strictly related to the underlying canopy architecture and its density (Georgiadis et al., 1996). Although the exact depth of this layer is difficult to identify because of the flow distortion effects induced by trees but it is assumed to be 1.5–2.5h (De Bruin and Moore, 1985; Cellier and Brunet, 1992; Wieringa, 1993). In Fig. 9b we see that this region is higher for the denser trees group (G2) than the sparse trees group (G1). The curvature of the profile while it tends to reach the logarithmic profile is more abrupt and bulged out in G2 than in G1. This was because in G2 the air tends to flow more above the trees than within the trees. Theoretically this makes the rate of increase in air velocity within the transition zone to be faster in the beginning and then later the rate of increase becomes back to normal. Garratt (1980) suggested that the gradient of wind speed in the *transition zone* over forest is well represented by:

$$\frac{\partial u}{\partial y} = \frac{u_*}{\kappa(y-y_0)}\Phi(y/y_0) \quad \text{for } y > y_0 \tag{15}$$

$$\text{where} \quad \Phi(y/y_0) = \gamma\exp\left[\gamma 1\left(\frac{y-y_0}{y_0}\right)\right], \quad \gamma = 0.5,\ \gamma 1 = 0.7 \tag{16}$$

The last inertial layer above the transition flow region is the logarithmic flow region. The airflow profile in this region is calculated using Eq. (1). The height at which the flow becomes logarithmic depends on the spatial structure and arrangement of the trees (Ni, 1997). The calculated profile in Fig. 9a and b are calculated using Eqs. (14), (15), and (1) for the canopy flow region, for the transition flow region and logarithmic region, respectively.

Fig. 10 shows the normalized velocity profiles in different regions across the domain on the same vertical plane at the wake as obtained from the cyclic simulation. As illustrated in the figure, this work showed vertical profiles of the average velocity for a row planted orchard is different across the row. The magnitude in fact depends on the direction of wind. Within the canopy height the velocity is lower in the row due to the resistance of the canopy than between the rows when the direction of wind is along the row. The average across the row lies between the two and this can also be obtained by the previous approaches that use the averaging procedure of Wilson and shaw (1977). But using the previous approaches it cannot be possible to show the differences across the raw due to the assumption of horizontal homogeneity. The results obtained were compared with previous works of Cionco and Ellefsen (1998) (CE1998), Pyles et al. (2004) (P2004) and Katul et al.

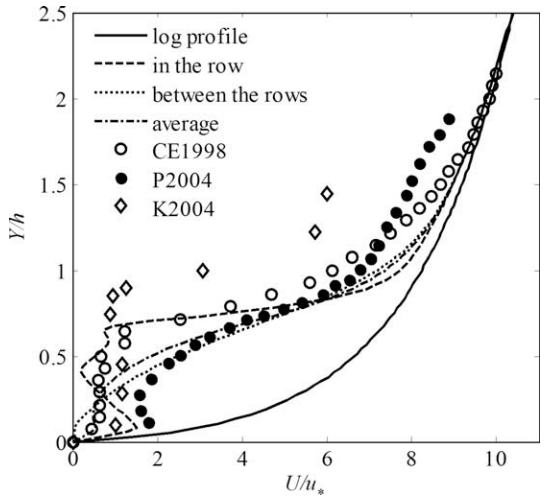

Fig. 10. Normalized vertical profiles of U at different horizontal positions across the wake representing typical flow profiles in the row and between the rows of an orchard and the average across the row compared with previous works; CE1998 (Cionco and Ellefsen, 1998), P2004 (Pyles et al., 2004) and K2004 (Katul et al., 2004).

(2004) (K2004). As described above the profile by Cionco and Ellefsen (1998) is a general vertical velocity profile expected over a canopy roughness. The P2004 (Pyles et al., 2004) is a canopy profile over old-growth temperate rainforest obtained using the UCD Advanced Canopy–Atmosphere–Soil (UCASD) algorithm. K2004 (Katul et al., 2004) is a profile over a forest canopy of hardwood. The normalized vertical velocity profiles are generally similar, qualitatively justifying the relevance of the present work to previous works.

Fig. 11 illustrates the vertical profiles of k of the present work simulated at $y_0 = 0.2$ mm with G1 trees compared with the profiles obtained by Wilson and Shaw (1977) (W1977), Wilson (1988) (W1988), Katul and Chang (1999) (KC1999) and Wilson et al. (1998) (W1998). Simulations done with the other roughness values of $y_0 = 0.1$ mm and 0.3 mm and that with the source sink terms in a detailed porous sub-domain created around the branches gave

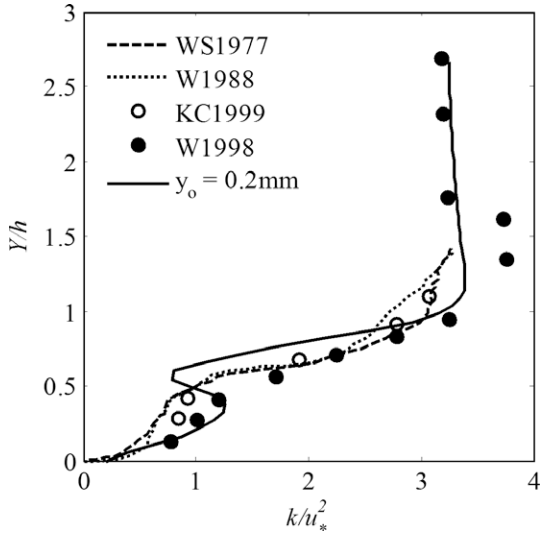

Fig. 11. Normalized vertical profiles of k horizontally averaged over position (B) obtained from cyclic simulations with the full scale trees of G1 and $y_0 = 0.2$ mm compared with previous works similar to U; W1977, W1988, KC1999 and W1998 are obtained from Wilson and Shaw (1977), Wilson (1988), Katul and Chang (1999) and Wilson et al. (1998), respectively.

similar profile as the one obtained with $y_0 = 0.2$ mm. Unlike the simulations in the wind tunnel, change of y_0 values in the full scale simulation did not give significant difference in the profiles of both k and U. Similar to the velocity profile the resemblance of the profiles of k of the present work with previous works rationalize the significance of this work.

5. Conclusions

The normalized vertical profiles of the horizontal velocity U both for the wind tunnel simulations revealed that there were good qualitative and quantitative agreements between observed and simulated results with minimum accuracies of 92%. In the wake region, though the qualitative agreement was quite acceptable, there were minor discrepancies within the canopy height. The measured velocity profiles were represented well with the trees as smooth wall boundaries. With regard to the turbulence properties, k and I, this work showed that the representation of the measured values by the model was not generally as good as that of U. Including tree surface roughness (y_0) and using source terms in a porous sub-domain around the branches simulated k and I better fit with measured values within the canopy height. Downstream of the trees the model well represented observed k and I within and above the canopy height except up to $0.2h$ from the ground. Among the several reasons, the differences between the measured and simulation results of all the parameters considered here especially the turbulence properties might be due to the complex phenomena of airflow within the complex 3D structure of the trees which could not be easily captured by steady state RANS equations and k-ε turbulence model which are mainly based on time and space averaging.

The differences in vertical profiles of the longitudinal velocities due to the differences in the spatial structures of the trees were also showed using two groups of trees with different spatial structure and density as compared with other works in the ABL. Three vertical regions of the velocity profiles were identified in all cases with similar qualitative shapes and some quantitative differences. This work showed that an increase in canopy density results in air velocity decrease in the lower canopy flow region and an increase above the canopy in the transition flow region. In the full scale simulation the changes in the roughness length, y_0 did not bring significant change in the values of both the velocity and turbulence properties as it did for the simulations that represent the wind tunnel.

In the model leaves were not included for two reasons; (1) for the sake of minimizing computational complexity, especially considering the problem their orientation can bring during meshing the fluid domain. (2) Excluding the leaves apart from minimizing computational complexity it may also help in an approach of 'worst case scenario' in drift prediction. Georgiadis et al. (1996) found that comparing the influence of the varying meteorological conditions and canopy characteristics on airflow, the geometry of the obstacle is the dominant factor.

With this numerical approach it was possible to predict airflow within the canopy in more details and to resolve the effects of the canopy elements to airflow by adding the 3D architecture into the model. The numerical approach presented here considers the real local effects of vegetation elements to airflow by introducing 3D canopy architecture into a simulation domain. With the estimation of the turbulence properties resolved, this approach can be an alternative for future applications in modelling pollutant transport, particle flow and deposition on plant canopies as well as for drift prediction. This can help to improve the design, calibration and operation of spraying equipments for effective application of pesticides to assure maximum protection with minimum drift (Endalew

et al., 2008). In the subsequent works the effects of leaves are included and the approach is extended to model the interaction of atmospheric and air-assisted orchard sprayer airflows with particle transport and deposition as well as drift prediction.

Acknowledgment

The Flemish and Belgium governments are gratefully acknowledged for their financial support (S-6209 and IWT-040708-05/591). Pieter Verboven is fellow of the Industrial Research Fund of the K.U.Leuven.

References

Albertson, J.D., Katul, G.G., Wiberg, P., 2001. Relative importance of local and regional controls on coupled water, carbon, and energy fluxes. Adv. Water Resour. 24, 1103–1118.

Ayotte, K.W., Finnigan, J.J., Raupach, M.R., 1999. A second order closure for neutrally stratified vegetative canopy flows. Boundary-Layer Meteorol. 90, 189–216.

Brown, R.B., Sidhamed, M.M., 2001. Simulation of spray dispersal and deposition from a forestry airblast sprayer – Part III: droplet trajectory model. Trans. ASAE 44, 11–17.

Cellier, P., Brunet, Y., 1992. Flux-gradient relationships above tall canopies. Agric. Forest Meteorol. 58, 93–117.

Cheng, Y., Lien, F.S., Yee, E., Sinclair, R., 2003. A comparison of large eddy simulations with a standard k-ε Reynolds-Averaged Navier–Stokes model for the prediction of a fully developed turbulent flow over a matrix of cubes. J. Wind Eng. Ind. Aerodyn. 91, 1301–1328.

Cionco, R.M., 1972. A wind profile index for canopy flow. Boundary-Layer Meteorol. 3, 255–263.

Cionco, R.M., Ellefsen, R., 1998. High resolution urban morphology data for urban wind flow modelling. Atmos. Environ. 32, 7–17.

Costes, E., Sinoquet, H., Godin, C., Kelner, J.J., 1999. 3D digitizing based on tree topology: application to study variability of apple quality within the canopy. Acta Hort. 499, 271–280.

Da Silva, A., Sinfort, C., Tinet, C., Pierrat, D., Huberson, S., 2006. A Lagrangian model for spray behaviour within vine canopies. J. Aerosol Sci. 37, 658–674.

De Bruin, H.A.R., Moore, C.J., 1985. Zero-plane displacement and roughness length for tall vegetation, derived from a simple mass conservation hypothesis. Boundary-Layer Meteorol. 31, 39–49.

Endalew, A.M., Hertog, M., Verboven, P., Baetens, K., Delele, M.A., Ramon, H., Nicolaï, B.M., 2006. 3D orchard canopy architectural modelling for use in airflow and drift predictions. Acta Hort. 718, 67–74.

Endalew, A.M., Hertog, M., Delele, M.A., Baetens, K., Vercammen, J., Gomand, A., Baelmans, M., Ramon, H., Nicolaï, B.M., Verboven, P., 2007. 3D measurement and representation of pear canopy for modelling air-assisted orchard spraying. Commun. Appl. Biol. Sci. Ghent Univ. 72 (1), 245–248.

Endalew, A.M., Hertog, M., Vercammen, J., Baetens, K., Delele, M.A., Blocken, B., Baelmans, M., Nicolaï, B.M., Ramon, H., Verboven, P., 2008. Using integrated 3D canopy architecture and porous media models for prediction of orchard pesticide applications. International advances in pesticide application. Aspect Appl. Biol., 425–432.

Faruquee, Z., Ting, D.S.-K., Fartaj, ., Barron, R.M., Carriveau, R., 2007. The effects of axis ratio on laminar fluid flow around an elliptical cylinder. Int. J. Heat Fluid Flow 28, 1178–1189.

Garratt, J.R., 1980. Surface influence upon vertical profiles in the atmospheric near surface layer. Quart. J. R. Meteor. Soc. 106, 802–819.

Georgiadis, T., Dalpane, E., Rossi, F., Nerozzi, F., 1996. Orchard-atmosphere physical exchanges: modelling the canopy aerodynamics. Acta Hort. 416, 177–182.

Godin, C., 2000. Representing and encoding plant architecture: a review. Ann. Forest Sci. 57, 413–438.

Gross, G., 1987. A numerical study of the air flow within and around a single tree. Boundary-Layer Meteorol. 40, 311–327.

Kaimal, J.C., Finnigan, J.J., 1994. Atmospheric Boundary Layer Flows: Their Structure and Measurement. Oxford University Press, New York. pp. 242 and 289.

Katul, G.G., Albertson, J.D., 1998. An investigation of higher-order closure models for a forested canopy. Boundary-Layer Meteorol. 89, 47–74.

Katul, G.G., Chang, W.H., 1999. Principal length scales in second-order closure models for canopy turbulence. J. Appl. Meteorol. 38, 1631–1643.

Katul, G.G., Mahrt, L., Poggi, D., Sanz, C., 2004. One- and two-equation models for canopy turbulence. Boundary-Layer Meteorol. 113, 81–109.

Lam, K., Lin, Y.F., 2008. Large eddy simulation of flow around wavy cylinders at a subcritical Reynolds number. Int. J. Heat Fluid Flow 29, 1071–1088.

Launder, B.E., Spalding, D.B., 1994. The numerical computation of turbulent flows. Comput. Meth. Appl. Mech. Eng. 3, 269–289.

Lee, X., 2000. Air motion within and above forest vegetation in non-ideal conditions. Forest Ecol. Manage. 135, 3–18.

Marcolla, B., Pitacco, A., Cescatti, A., 2003. Canopy architecture and turbulence structure in a coniferous forest. Boundary-Layer Meteorol. 108, 39–59.

Meyers, T.P., Paw, U.K.T., 1986. Testing of a higher order closure model for air flow within and above plant canopies. Boundary-Layer Meteorol. 37, 297–311.

Muhar, A., 2001. Three-dimensional modelling and visualisation of vegetation for landscape simulation. Landscape Urban Plan. 54, 5–17.

Ni, W., 1997. A coupled transilience model for turbulent air flow within plant canopies and the planetary boundary layer. Agric. Forest Meteorol. 86, 77–105.

Poggi, D., Porporato, A., Ridolfi, L., Albertson, J.D., Katul, G.G., 2004. The effect of vegetation density on canopy sublayer turbulence. Boundary-Layer Meteorol. 111, 565–587.

Prusinkiewicz, P., Lindenmayer, A., 1996. The Algorithmic Beauty of Plants. Springer-Verlag, New York. p. 240.

Pyles, R.D., Paw, U.K.T., Falk, M., 2004. Directional wind shear within an old-growth temperate rainforest: observations and model results. Agric. Forest Meteorol. 125, 19–31.

Raupach, M.R., Shaw, R.H., 1982. Averaging procedures for flow within vegetation canopies. Boundary-Layer Meteorol. 22, 79–90.

Sanz, C., 2003. A note on k-ε modelling of vegetation canopy air-flows. Boundary-Layer Meteorol. 108, 191–197.

Shaw, R.H., 1977. Secondary wind speed maxima inside plant canopies. J. Appl. Meteorol. 16, 514–521.

Sievänena, R., Nikinmaa, E., Nygren, P., Ozier-Lafontaine, H., Perttunen, J., Hakula, H., 2000. Components of functional–structural tree models. Ann. Forest Sci. 57, 399–412.

Sinoquet, H., Rivet, P., Godine, C., 1997. Assessment of the three-dimensional architecture of walnut trees using digitizing. Silva Fennica 31 (3), 265–273.

Versteeg, H.K., Malalasekera, W., 1995. An introduction to computational fluid dynamics. The Finite Volume Method. Prentice-Hall, Englewood Cliffs, NJ. pp.257.

Walklate, P.J., Weiner, K.-L., Parkin, C.S., 1996. Analysis of and experimental measurements made on a moving air-assisted sprayer with two-dimensional air-jets penetrating a uniform crop canopy. J. Agric. Eng. Res. 63, 365–378.

Walklate, P.J., Cross, J.V., Richardson, G.M., Murray, R.A., Baker, D.E., 2002. Comparison of different spray volume deposition models using LIDAR measurements of apple orchards. Biosyst. Eng. 82, 253–267.

Wieringa, J., 1992. Updating the Davenport roughness classification. J. Wind Eng. Ind. Aerodyn. 41, 357–368.

Wieringa, J., 1993. Representative roughness parameters for homogeneous terrain. Boundary-Layer Meteorol. 63, 323–363.

Wilson, J.D., 1988. A second order closure model for flow through vegetation. Boundary-Layer Meteorol. 42, 371–392.

Wilson, J.D., 1989. Turbulent transport within the plant canopy, in estimation of areal evapotranspiration. IAHS 177, 43–80.

Wilson, N.R., Shaw, R.H., 1977. A higher order closure model for canopy flow. J. Appl. Meteorol. 16, 1197–1205.

Wilson, J.D., Finnigan, J.J., Raupach, M.R., 1998. A first-order closure for disturbed plant-canopy flows, and its application to winds in a canopy on a ridge. Quart. J. R. Meteorol. Soc. 124, 705–732.

Xu, Z.G., Walklate, P.J., McLeod, A.R., 1997. Numerical study of a full-size free-air fumigation system. Agric. Forest Meteorol. 85, 159–170.

Zeng, P., Takahashi, H., 2000. A first-order closure model for the wind flow within and above vegetation canopies. Agric. Forest Meteorol. 103, 301–313.